Thermal boundary layers and heat flux in turbulent convection: The role of recirculating flows

T. H. Solomon* and J. P. Gollub
Department of Physics, Haverford College, Haverford, Pennsylvania 19041
and Department of Physics, University of Pennsylvania, Philadelphia, Pennsylvania 19104
(Received 19 December 1990)

We experimentally examine the hypothesis that the scaling of the Nusselt number Nu (nondimensional heat flux) with Rayleigh number Ra in turbulent thermal convection is affected by large-scale flows near and within the boundary layers. The natural flows are enhanced artificially by a moving layer of mercury beneath the convecting fluid. Recirculating large-scale flows are thereby induced near the lower thermal boundary layer, and Nu is enhanced by as much as 70%. The response to forcing allows a determination of the large-scale flows needed to account for the observed scaling of Nu with Ra in the *unperturbed* situation. The required flows are found to be comparable to those present naturally, about 1.5 mm/s at $\mathrm{Ra}=10^8$ and a Prandtl number near 5. The experiments thus indicate that Nu is at least largely determined by a balance between diffusion of heat into the boundary layers and advection from them by large-scale flows. In an appendix, the form of the temperature probability distribution in the interior is shown to be related to the coherence of the thermal plumes.

I. INTRODUCTION

The importance of thermal boundary layers in turbulent Rayleigh-Bénard convection is well documented. The heat flux through the fluid is limited by the thickness of the boundary layers, in which the vertical temperature difference is predominantly concentrated. In addition, eruptions of hot and cold fluid from the boundary layers drive the turbulent flow and determine the temperature statistics in the central region of the flow. For these reasons, much can be learned about turbulent convection by studying the properties of the boundary layers.

The variation of the heat flux with the Rayleigh number Ra (the nondimensional vertical temperature difference) can be roughly predicted[1,2] by assuming that the diffusive boundary layers are marginally stable at a thickness δ_b that depends only on the temperature drop. However, the resulting prediction that the Nusselt number Nu (the nondimensional heat flux) varies as Ra^β with $\beta=\frac{1}{3}$ is not in good agreement with many experiments (see Sec. II), and this fact has led to the suggestion that interactions of the boundary layer with the temperature or velocity field are significant. Experiments by Krishnamurti and Howard[3] and later thorough studies by Sano, Wu, and Libchaber[4] and Asaeda and Watanabe[5] showed that persistent larger-scale flows occur in turbulent thermal convection. These "winds" may play an important role in determining the heat flux, either by modifying the stability condition for δ_b or by advecting heat directly from the boundary layers. Castaing *et al.*[6] and Zaleski[7] predicted that shearing of the boundary layer by horizontal flows would increase the thickness δ_b at which the boundary layers become unstable, thereby decreasing the heat flux. A somewhat different approach was taken subsequently by Shraiman and Siggia,[8] who predicted that δ_b is governed not by marginal stability, but by a balance between the diffusive heat flux into the boundary layers and the flux advected from the boundary layers by turbulent flows.

These developments stress the fundamental importance of understanding the role of flows near the boundary layers in turbulent convection. Furthermore, convective flows in most realistic situations (e.g., in the atmosphere, oceans, or stellar interiors) are superimposed on a turbulent background and are frequently affected by boundary-layer shear. Motivated by these issues, we have studied the effects of imposed recirculating flows on the properties of the boundary layers and the overall flow. Flows in the vicinity of the lower thermal boundary layer are enhanced artificially by placing the convecting fluid above a layer of mercury which can be driven electromagnetically to provide a moving boundary condition. By examining the response to such "imposed winds," we learn how spontaneous large-scale flows affect the heat flux in the unperturbed case.

Several distinct types of forcing were employed in these experiments. In a previous paper,[9] we described the effects on δ_b and on the heat flux of induced flows that are entirely *horizontal* and confined to the thermal boundary layer. Ideally, such horizontal flows, which are created by oscillatory or ac forcing, do not result in *advective* heat flux from the boundary layers, and are expected to affect the total heat flux only if δ_b is governed by marginal stability and if the stability is shear dependent. In that study, we found that the imposed horizontal shear flows did not affect the heat flux substantially, although significant changes in the frequency and size of thermal eruptions were observed.

The present paper extends the previous work to the case of *recirculating* flows (induced by steady or dc electromagnetic forcing), which are expected to increase the advection of heat from the boundary layer, much as the

natural large-scale flows presumably do. We demonstrate that in the presence of recirculating flows of sufficient magnitude, the thickness of the boundary layer is governed by a balance between diffusion and advection ("flux balance"), rather than by marginal stability. The quantitative effects of advective flows on the dimensionless heat flux Nu are measured, and a simple scaling relation is found to describe the variation of Nu with Ra and the recirculating flow v_s. The large-scale flow required to account for the deviation of the unperturbed Nu with Ra is approximately 1.5 mm/s at $\mathrm{Ra}=10^8$, a value consistent with flows naturally present. The external flow also creates an asymmetry between the two boundary layers and shifts the center temperature. This shift is measured and shown to be consistent with the change in heat flux.

We also present (in the Appendix) results relevant to understanding the differences between the statistics of "soft" and "hard" turbulence, two convective regimes discovered by Heslot, Castaing, and Libchaber.[10] The transition between these two regimes is characterized by a change in the temperature probability distribution function (PDF) in the interior from Gaussian (for soft turbulence) to exponential (for hard turbulence). Further experiments[11,12] indicated that this transition may be caused by an instability leading to the propagation of thermal waves in the boundary layers. Here we show that the coherence of plumes affects the form of the PDF's.

The body of the paper is organized as follows. Section II contains a summary of theories and experiments that are relevant to our studies. The experimental techniques are explained in Sec. III. Measurements of the heat flux and temperature shifts are presented in Sec. IV and analyzed in Sec. V. In the concluding section (Sec. VI), we discuss the implications of our results for unperturbed convection. Finally, the temperature statistics are discussed in the Appendix.

II. BACKGROUND: HEAT FLUX AND SCALING LAWS

The strength of the heating in Rayleigh-Bénard convection is parametrized nondimensionally by the Rayleigh number $\mathrm{Ra}=\alpha g\Delta T d^3/\kappa\nu$, where g is the gravitational acceleration, d is the depth of the fluid layer, ΔT is the vertical temperature difference, and α, κ, and ν are the expansion coefficient, thermal diffusivity, and kinematic viscosity of the fluid. In turbulent convection at large Ra, the vertical temperature difference is concentrated predominantly in thin transition regions (boundary layers) with thickness δ_b near the top and bottom surfaces of the convecting layer. The transport of heat through these boundary layers is diffusive, since the velocity must drop to zero at the walls. With an appropriate definition for δ_b, this diffusive flux is given by

$$H=\frac{k\Delta T}{2\delta_b}\ , \tag{1}$$

where k is the thermal conductivity of the fluid. If the central region of the flow is assumed to be isothermal, the *total* convective heat flux is given by Eq. (1). The heat flux is usually expressed nondimensionally as the Nusselt number Nu, defined as the ratio of the total heat flux to the conductive heat flux that would be found in the absence of a flow. With the assumptions given above, $\mathrm{Nu}=d/2\delta_b$, and the problem is reduced to the determination of δ_b.

A. Marginal stability approaches

Malkus[1] and Howard[2] proposed that δ_b is governed by marginal stability. If the instantaneous thickness δ is less than a critical value δ_b, the thermal boundary layers are stable and diffusion of heat into the boundary layers [Eq. (1)] causes δ to increase. If $\delta>\delta_b$, the boundary layers are unstable and erupt, throwing off plumes of hot or cold fluid and decreasing δ. In the steady state, the two processes (diffusion of heat into the boundary layers and thermal eruptions) balance, fixing δ at δ_b. Malkus and Howard predicted that the boundary layer stability would depend only on a Rayleigh number based on δ_b (assuming a temperature difference $\Delta T/2$). The existence of a stability condition which does not depend on the cell depth d requires that the heat flux vary as $\mathrm{Nu}\sim\mathrm{Ra}^\beta$, with $\beta=\frac{1}{3}$. If it is further assumed that the critical boundary-layer Rayleigh number is merely the Rayleigh number Ra_c for the onset of convection, then the heat flux is given by the relation

$$\mathrm{Nu}_{\mathrm{cl}}=0.40\left[\frac{\mathrm{Ra}}{\mathrm{Ra}_c}\right]^{1/3}\ . \tag{2}$$

These early scaling predictions with $\beta=\frac{1}{3}$, which are sometimes called "classical" theories (hence the subscript "cl"), were all based on the assumption that δ_b does not depend upon d. The interaction of the boundary layers with the velocity field, which *does* depend on d, was therefore presumed negligible. Various experiments have studied the scaling of Nu with Ra in turbulent thermal convection.[10,13–17] Scaling exponents determined in these studies are approximately 0.28–0.29, values that are consistently (and significantly) lower than the classical prediction of $\frac{1}{3}$. The most precise measurement of the "nonclassical" scaling exponent was made recently by Heslot, Castaing, and Libchaber,[10] who found $\beta=0.282$. (However, Goldstein, Chaing, and See[18] suggested that the reduced exponent may be due to the limited range in Ra of some previous experiments. They described an experimental study of high Ra electrically induced *mass* convection, in which an exponent 1/3 was found.)

Modifications to the marginal stability theories were made by Castaing *et al.*[6] to explain the experimental results. They proposed that horizontal winds shear the boundary layer and increase the thickness δ_b at which the boundary layer is marginally stable (shear-induced stability). Having established a d dependence for δ_b, Castaing *et al.* developed a "mixing layer" theory in which the acceleration of thermal plumes (whose sizes were assumed to grow linearly with δ_b) from the boundary layers to the average central flow velocity is used to determine δ_b. They predicted a scaling exponent $\beta=\frac{2}{7}$, in good agreement with the experiments.

In a previous paper,[9] we reported direct experimental

tests of this hypothesis of shear-induced stabilization of the thermal boundary layers in turbulent convection. Horizontal flows were induced in the vicinity of the lower thermal boundary layer, which enhanced the boundary-layer shear by an order of magnitude over the unperturbed case. The enhanced shear was observed to inhibit aggregation of hot eruptions in and near the boundary layer and to increase the frequency of thermal plumes substantially. However, no significant change in Nu was observed. These experimental results were interpreted to mean that *if δ_b is governed by marginal stability, it is unlikely that shearing of the boundary layer by purely horizontal winds could be responsible for the nonclassical scaling exponent.* However, the effect of shear depends on parameters in a fairly complex way, as discussed by Zaleski.[19] The possible significance of flows with recirculation was not addressed in our previous paper.

B. Recirculating flows and flux-balanced boundary layers

Large-scale recirculating flows have been studied recently in some detail. Sano, Wu, and Libchaber[4] found that convection at large Ra ($>10^7$) in a cell with aspect ratio near unity is characterized by a persistent, cellular net wind that rises at one side of the cell and descends at the opposite side. Asaeda and Watanabe[5] showed experimentally that convection cells with large aspect ratios also have large-scale flows, with fluid rising from and descending into the lower boundary layer in long, coherent, slowly evolving sheets.

A recent explanation of the heat-transport experiments by Shraiman and Siggia[8] takes into account direct advection of heat from the boundary layers by large-scale recirculating flows, such as those observed by Sano *et al.* and by Asaeda and Watanabe. The thermal boundary layer is assumed to be nested within the viscous sublayer of a turbulent boundary flow, an assumption that should be valid at Rayleigh numbers that are sufficiently high to create the assumed turbulent flow, but not so high as to make the viscous sublayer of the turbulent flow thinner than the *thermal* boundary layer. The known velocity field describing a viscous sublayer is used to calculate the heat flux advected from the boundary layer by the large-scale flow. The balance between this advective heat flux and the diffusive heat flux [Eq. (1)] determines δ_b and Nu. The result is a scaling prediction with a nonclassical exponent in good agreement with experiment. No assumptions of stability are required with this "flux-balanced" approach. (Since advection limits the growth of δ_b, the boundary layer need never exceed the marginally stable thickness.) Furthermore, no assumptions of any kind are made about thermal plumes.

III. EXPERIMENTAL METHODS

A. Forcing mechanism

The forcing in this experiment is applied to the lower boundary layer of the convecting fluid (water) by a layer of mercury that forms the bottom of the convection cell. A horizontal flow induced in the mercury shears the boundary layer and enhances the flow velocities at the bottom of the cell. By varying the magnitude, time dependence, and spatial structure of the mercury flow, a variety of perturbations can be applied to the convecting fluid.

The mercury flow is induced by a nonintrusive magnetohydrodynamic technique.[20,21] A spatially varying magnetic field is applied to the mercury layer by a configuration of alternating permanent magnets (0.5-in.-diam neodymium-iron-boron magnets) located underneath the mercury layer (Fig. 1). A uniform electric current (0–10 A) passing horizontally through the mercury interacts with the magnetic field via the Lorentz force. The spatially varying magnetic forces induce a (predominantly) horizontal cellular flow in the mercury (a collection of vortices with vertical axes) with an amplitude that depends on the current and a spatial organization that depends on the magnet configuration. Two configurations are used in this experiment. The four-magnet arrangement of Fig. 1(a) produces a single large vortex in the mercury ("single-vortex forcing"). Most of the experiments reported in this article utilize a close-packed 6×6 square array of alternating magnets [Fig. 1(b)] to induce a pattern of small vortices in the mercury ("many-vortex forcing"). The magnet array has dimensions 3×3 in.^{2} while the mercury layer above has dimensions 2.5×2.5 in.^{2} The resulting flow in the mercury is a well-ordered 4×4 array of vortices with alternating directions of circulation (Fig. 2). At the highest forcing currents used in the experiment (5–10 A), the vortex flow is slightly time dependent. Individual vortices fluctuate in magnitude (with a time scale of a few seconds) and also move laterally to some extent, although no significant vortex merging is observed.

A "mirror votex" in the water is created above each vortex in the mercury. In addition (and most important-

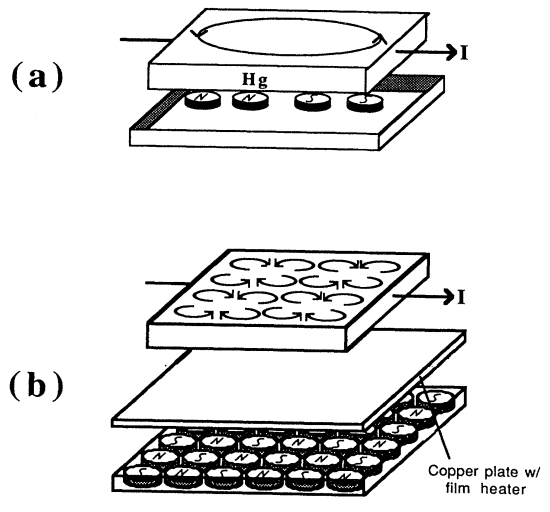

FIG. 1. Exploded view of the bottom of the convection apparatus, showing magnetohydrodynamic forcing mechanisms. (a) Single-vortex forcing. (b) Many-vortex forcing. The thin copper plate used to heat the mercury is shown in (b), but not in (a).

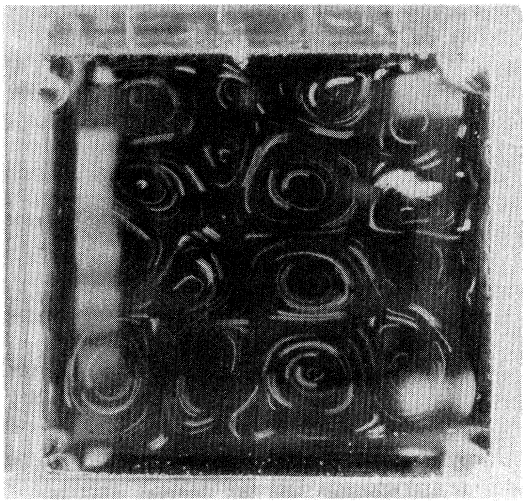

FIG. 2. Time exposure of the mercury flow with many-vortex forcing. The maximum velocity, as determined by particle streak photography, is 1.6 cm/s.

ly) secondary flows are induced with recirculating winds in the convecting fluid[22] (Fig. 3). To see the origin of this secondary flow, note that a mirror vortex just above the mercury-water interface creates a radial pressure gradient that pumps fluid outward near the interface. This outward flow turns upward at the edges of the mirror vortex, inward in the interior of the fluid layer at a height of the order of the diameter of the mirror vortex, and downward into the center of the mirror vortex. These secondary recirculating flows increase the advective transport of heat from the lower boundary layer (as is demonstrated in Sec. IV).

Numerical computations were done in order to estimate the characteristics of the secondary flow.[23] The amplitude of the secondary-flow field is found to scale roughly linearly with the maximum horizontal velocity v_f of the forcing vortices. For the many-vortex forcing configuration, the maximum secondary vertical velocity v_s is approximately 20% of v_f in the relevant range of forcing velocities. Because of this linear dependence, we can parametrize the imposed enhancement of boundary-layer velocities (both horizontal and vertical) by either v_f or v_s when discussing scaling laws.

B. Convection apparatus

A diagram of the apparatus used in our studies of turbulent convection is shown in Fig. 4. A Plexiglass box with $\frac{3}{4}$-in-thick walls encloses both the convecting fluid (water at temperatures between 30 and 40°C, Prandtl number Pr$\sim$5) and a 7-mm-thick mercury layer at the bottom. The convecting layer is 6.35×6.35 cm^2 horizontally; depths of both 4.0 and 9.0 cm are used to extend the accessible range in Ra. A temperature difference $\Delta T\sim1-5$ °C is imposed across the convecting fluid, stable to ~0.01 °C. For these experiments, Ra is varied between 10^6 and 10^8.

Two 7-mm-high nickel electrodes are embedded in the bottom of the Plexiglass box on two opposing sides. On each side, four metal rods 1.5 mm in diameter pierce the Plexiglass and establish electrical connections between the electrode and a 50-A power supply. The electrode surfaces are polished and electroplated with a thin layer of gold. This is done to improve the wetting of the nickel surfaces by the mercury,[24] and hence reduce the contact resistance. Furthermore, with the addition of two pieces of gold-plated nickel foil 7-mm high on the remaining two sides, the mercury interface can be prevented from curving downward at the edges of the cell.

The temperature difference ΔT is maintained by controlling the temperatures of the mercury layer and a sapphire window at the top. The mercury temperature is

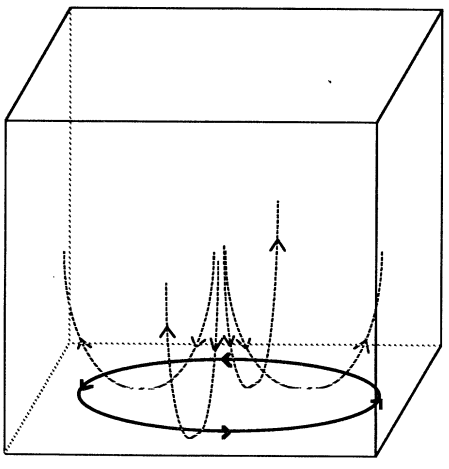

FIG. 3. Diagram of the secondary flow (dotted lines) associated with a mirror vortex (bold line). The secondary flow moves downward in the center of the vortex and upward at the edges of the vortex.

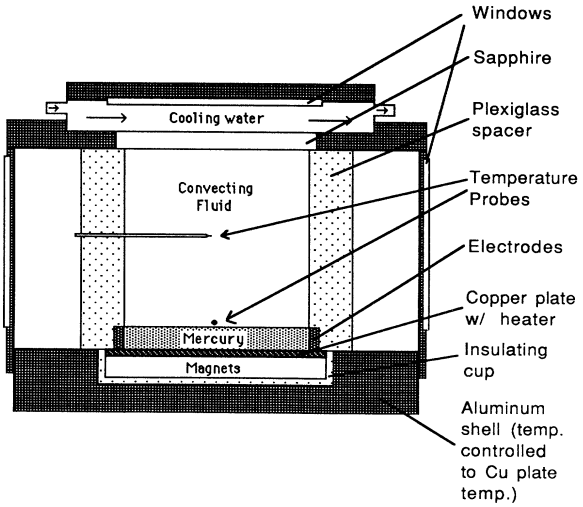

FIG. 4. Diagram of the convection apparatus. The gap between the plexiglass spacer and the outer shell is filled with styrofoam when quantitative measurements are made.

controlled electronically by means of a thin copper plate below the mercury to which is laminated a film heater and a small thermister (0.5 mm in diameter). Three thermisters are inserted into the mercury at three of the four corners to monitor its temperature. The temperature of the sapphire window is maintained by a regulated water flow pumped from a temperature-controlled reservoir through a compartment above the sapphire window. Thermisters are inserted into the flow immediately before and after the cell apparatus to monitor the temperature of the sapphire. The vertical heat flux through the cell is determined from the power required to keep the mercury at a constant temperature (with corrections for Joule heating of the mercury from the electrical current). Measurements of Nu are stable to within $\sim 2\%$.

Two small (0.5-mm diameter) glass-encapsulated thermisters are inserted into the convecting fluid to obtain local measurements of the temperatures. One probe is located 2–3 mm above the mercury-water interface (just above the bottom thermal boundary layer), centered laterally, and the other is located at the midheight of the cell. The time constant of these thermisters is 18 msec, an order of magnitude faster than the shortest time scales of the convective flow.

An aluminum block forms the bottom of the convection apparatus. A 3.5-in.-square section is milled out of the surface of the block, in which the magnet arrangement and the copper plate (with heater) are placed. The copper plate and magnets are separated from the bottom block by an insulating cup of Plexiglass $\frac{1}{4}$ in thick. In addition, the block is separately controlled at the temperature of the mercury. The insulating cup and the aluminum block together minimize heat leakage from the copper plate through the bottom.

The aluminum block and the Plexiglass box containing the convecting fluid are surrounded by an insulating shell as an additional temperature buffer between the convection cell and the room. Plexiglass windows on all four sides allow optical access to the inside of the convection cell. When quantitative measurements are made of the heat flux and the center temperatures, the gap between the Plexiglass box and the aluminum shell is filled with shredded styrofoam to reduce the heat leakage through the side walls.

C. Interfacial contamination

Cleanliness is particularly important in this experiment. Impurities in the convection cell are adsorbed at the mercury-water interface, forming a thin, tenacious, but invisible skin that can prevent the transmission of shear stresses across the interface and thereby make the external forcing ineffective. This problem is particularly acute because the mechanical properties of the interface can be affected by a *monolayer* of adsorbed impurity. (See Refs. 25 and 26 for information on this phenomenon.) To minimize this problem, the cell is cleaned carefully before use, and liquid chromatography grade water is used for the convecting fluid. In addition, the interface is cleaned periodically with an interface cleaner consisting of a syringe fitted with a flexible hose and a long piece of stainless-steel tubing.[27]

D. Flow characterization

Qualitative observations of the temperature field of the convecting fluid are important for interpreting the quantitative measurements. In these experiments, we employ a recent technique[28] that uses thermochromic liquid-crystal (TLC) microspheres[29] to visualize the temperature field. Details of this technique have been presented in Ref. 9, along with examples of TLC images.

The velocities of the mercury-forcing flow are measured with particle-tracking techniques.[30] Small (~ 100 μm), hollow, ceramic spheres are injected onto the interface. These particles spread out over the mercury surface and follow the movement of the interface (see Fig. 2). A camera mounted above the cell is used to photograph the movements of the particles. The time of the exposure (critical for determining the velocities) is set by a computer-controlled electromechanical shutter at the focal point of a lamp (75-W halogen bulb or xenon-argon arc lamp) that illuminates the interface.[23] The particle streaks are digitized by projecting the image onto a digitizing tablet and recording the endpoints of the streaks with the stylus. Once digitized, the streak lengths are computed, and the velocity distribution is determined by dividing by the exposure time. For the single-vortex configuration, the forcing is characterized quantitatively by the maximum horizontal velocity v_f of the mercury, and by the maximum vertical component of the induced secondary flow, $v_s \cong 0.20 v_f$. (The maximum *radial* component of the induced flow is comparable to v_s; the *tangential* velocity, which is of course equal to v_f, is larger but does not promote heat transfer.)

The external forcing dominates the velocity field in the vicinity of the lower boundary layer throughout these experiments. The forcing velocity v_f is in the range 1.5–5 cm/s, so v_s is in the range 0.3–1 cm/s in these studies. By comparison, the unperturbed root-mean-square horizontal velocity above the lower boundary layer (estimated with laser Doppler velocimetry and by particle tracking) is approximately 0.1–0.2 cm/s at $\mathrm{Ra} \sim 10^8$. The induced flow, when present, is therefore always substantial in comparison with the natural large-scale flow.

E. Effects of interfacial deformations

Deformations of the mercury-water interface can result either from vibrations of the table on which the equipment is mounted (up to ~ 0.1–0.2 mm), or from rotational effects of the forcing vortices. Deformations from rotation are up to ~ 0.5 mm at the largest forcing velocity (for single-vortex forcing). Two types of tests demonstrate that these interfacial deformations do not affect the heat transfer significantly. When contamination is sufficient to form a skin on the mercury surface, the mercury flows do not affect the velocities in the convecting layer but still deform the interface. No changes in Nu are observed in these cases. Tests are also made by agitating the equipment with a mechanical pump placed on the optical table to produce deformations up to 1–2 mm.

Again, and perhaps surprisingly, no significant changes in Nu are observed.

IV. RESULTS

A. Unperturbed convection

We start with a discussion of the behavior of the flow in the absence of boundary forcing. A plot of Nu versus Ra in the unperturbed case for $1\times10^6<\mathrm{Ra}<2\times10^8$ is shown in Fig. 5, along with the experimental results of Ref. 14, which also used water as the convecting fluid. (The results of Refs. 13, 15, 16, and 17 agree with those of Ref. 14.) There is a weak dependence of Nu on the aspect ratio.[8,15] This dependence is not significant for aspect rations greater than about 1.5, as was shown by Chu and Goldstein.[14] However, the data for the tall cell (aspect ratio 0.71) is shifted upward slightly ($\sim7\%$) by this effect. We have corrected for this aspect ratio dependence in Fig. 5 by dividing the Nu data for this cell by 1.07. It should be noted that the scaling exponents obtained by fitting the data for each depth independently agree with each other.

Our results are well described by the scaling relation

$$\mathrm{Nu}=0.137\mathrm{Ra}^{0.275}, \tag{3}$$

though the range is limited compared to what can be achieved in helium. The scaling exponent $\beta=0.275\pm0.007$ agrees well with that of Ref. 14, but the proportionality constant is slightly lower (24%). The difference in this constant may be due to the use of mercury and sapphire as boundaries rather than copper, which has a higher thermal diffusivity. The difference is not due to the use of a stress-free boundary, demonstrated by the observation that Nu remains unchanged when the interface forms a skin. The consistency of our measurements of β with those of previous experiments indicates that this system is suitable for studying the scaling of the heat flux in turbulent convection.

Note that at $\mathrm{Ra}=10^8$, $\mathrm{Nu}=1.52\mathrm{Nu}_{\mathrm{cl}}$, so the heat flux is *higher* than the classical prediction at this Ra, though the exponent is less. The two curves (Nu versus Ra and $\mathrm{Nu}_{\mathrm{cl}}$ versus Ra) cross at much higher Ra.

B. Single-vortex forcing

For simplicity, we first describe the effects of single-vortex forcing [Fig. 1(a)] at Rayleigh numbers between 10^6 and 10^8. The most striking effect is the suppression of eruptions of the lower boundary layer. Figure 6 illustrates this behavior (as viewed with liquid-crystal visualization). Hot fluid from the lower boundary layer is advected up the sides of the cell by the secondary flow. The lower thermal boundary layer remains stagnant. The upper boundary layer continues to erupt, but the eruptions are slowly evolving and less frequent than in the unperturbed case. The resulting cool plumes are unopposed, since there are no warm eruptions creating vertical flows near the middle of the upper boundary layer. As a result, these plumes often span the entire height of the cell, even at the largest Rayleigh numbers studied ($\mathrm{Ra}\sim10^8$, $d=9.0$ cm).

The suppression of eruptions by the large-scale flow is also clearly manifested in local temperature measurements near the lower boundary layer, as shown in Fig. 7 for $\mathrm{Ra}=5.2\times10^7$. In the unperturbed case [Fig. 7(a)], warm eruptions from the lower boundary layer result in temperature fluctuations up to 0.8 °C. These fluctuations should be compared to the mean (unperturbed) temperature drop across the lower boundary layer $\Delta T/2=1.1$ °C. With forcing [Fig. 7(b)], the fluctuations are much less, due to the absence of warm eruptions. The temperature at the probe then remains close to the average interior temperature (35.90 °C).

The cessation of warm eruptions from the lower

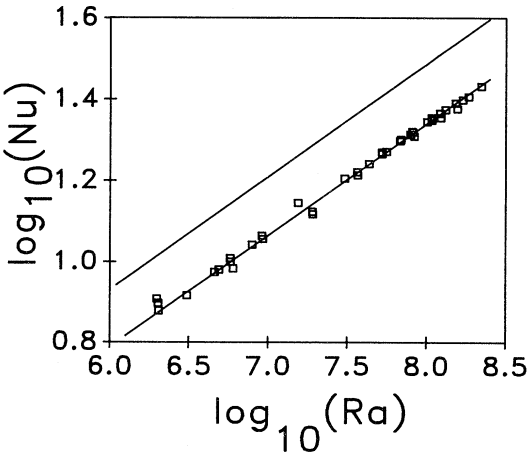

FIG. 5. Scaling of the Nusselt number Nu with Rayleigh number Ra for unforced convection, along with a power-law fit [Eq. (3)]. The top curve is the experimental result of Chu and Goldstein.

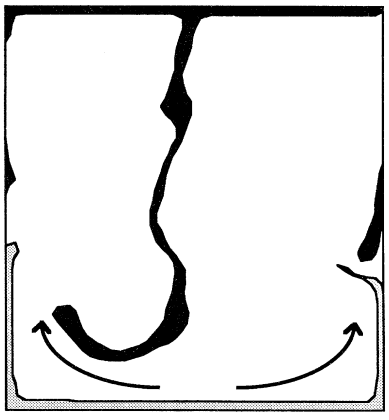

FIG. 6. Example of the dominant thermal features with single-vortex forcing. This sketch is based on liquid-crystal thermography. The secondary flow advects warm fluid (light shading) up along the side walls of the cell and creates a non-bursting lower boundary layer. Cool thermal plumes (dark shading) falling from the top are unopposed and frequently span the full height of the cell.

boundary layer implies that the advective heat flux from the boundary layer due to the secondary flow is large enough to balance the diffusive flux into the layer. As a result, the boundary-layer thickness does not grow to the marginally stable value. The ability of recirculating flows in *unperturbed* convection to control the boundary-layer thickness is discussed in Sec. VI.

Substantial enhancements in the heat flux (up to 50%) are observed with single-vortex forcing, due to advection of heat from the boundary layer by the secondary flow. However, for quantitative studies we use the many-vortex configuration.

C. Many-vortex forcing

We utilize many-vortex forcing (4×4 array of secondary vortices) for quantitative measurements of the enhanced heat flux, to minimize the possibility of finite-size effects associated with the lateral boundaries of the cell. The qualitative effect of many vortex forcing (Fig. 8) is similar in many respects to that of single-vortex forcing except that the advective plumes occur at the boundaries between adjacent secondary vortices, rather than only at the side walls. The plumes are fairly steady, apparently changing when the vortices in the mercury fluctuate in amplitude or shift in location.

Significant enhancement (up to 70%) in the heat flux is observed with this forcing configuration (Fig. 9). The magnitude of the enhancement decreases with increasing Ra at constant cell depth d. This Rayleigh number dependence is visible if Nu is plotted logarithmically versus Ra *with constant forcing* (Fig. 10). In this figure, we account for variations in cell depth d by holding

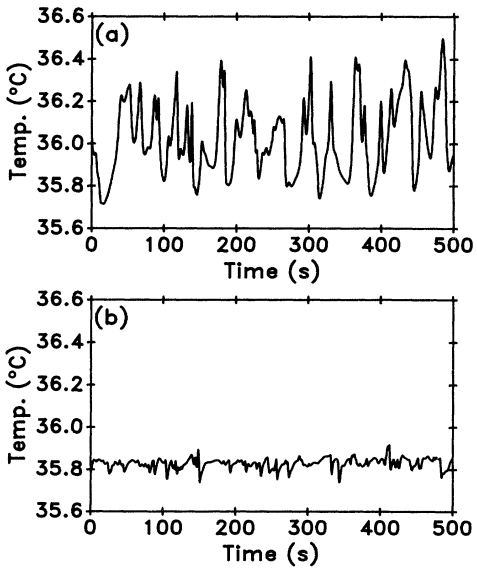

FIG. 7. Temperature time series measured at the lower probe, at Ra=5.2×10^7. (a) Unperturbed convection. (b) Time-independent forcing by a single vortex with $v_f=3.2$ cm/s. Warm temperature excursions are almost completely absent in (b), indicating a nonbursting lower boundary layer.

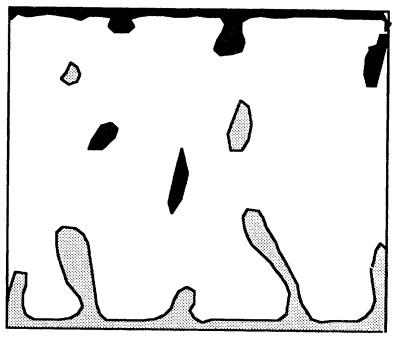

FIG. 8. Cartoon sketch of the temperature field with many-vortex forcing, as a function of the forcing velocity v_f. Secondary flows advect heat upward at the boundaries between forcing vortices.

$v_f d/\kappa$ constant, since convective velocities scale with κ/d.[31,32]

The advective heat flux from the lower boundary layer increases the center temperature (Fig. 11). This shift reflects the asymmetry between the upper and lower boundary layers when the system is forced from below. We discuss these temperature shifts quantitatively in the next section.

V. DATA ANALYSIS—MANY-VORTEX FORCING

A. Temperature asymmetry

It is necessary to correct for the fact that, in these experiments, we have perturbed only the lower thermal boundary layer. To understand the possible role of recirculating flows in unperturbed convection, we need to determine the relation between Nu and Ra with *both* boundary layers subjected to the same recirculating flows. This relation can be obtained from the experimental data

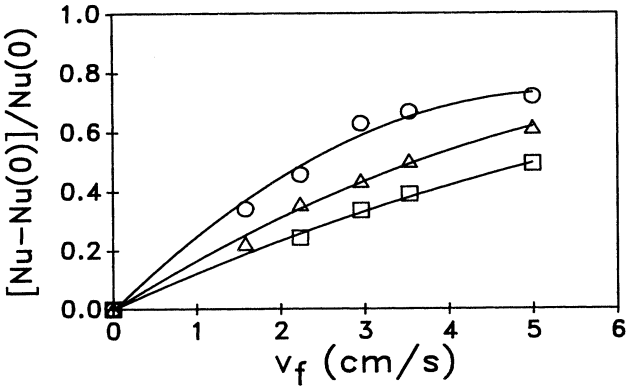

FIG. 9. Enhancement of the Nusselt number Nu by many-vortex forcing: Ra=1.8×10^7 (○), Ra=5.0×10^7 (△), Ra=1.0×10^8 (□). Curves are drawn through the data to guide the eye.

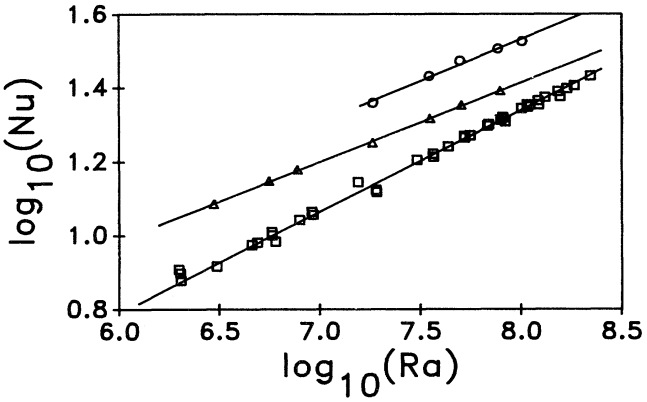

FIG. 10. Scaling of Nu with Ra, with nondimensional forcing $v_f d/\kappa$ held constant at the following values: zero (□), 9.4×10^3 (△), and 3.0×10^4 (○). The heat flux is increased (and the slope reduced) by the forcing (upper two curves).

difference across the boundary layers, rather than the temperature field. As is shown below, however, the averaging is not a problem with this boundary-layer analysis.

We illustrate this approach this approach by analyzing the temperature shift data of Fig. 11 and the heat flux across the upper (unperturbed) boundary layer. We can show that the unperturbed scaling laws are consistent with an analysis of the upper (unperturbed) boundary layer, even when the bottom boundary layer is perturbed. With $\mathrm{Nu}(v_s=0)=A\,\mathrm{Ra}^{\beta}$, the heat flux in the unperturbed case is given by

$$H(0)=\frac{k\Delta T}{d}\mathrm{Nu}(0)=A\frac{k\Delta T}{d}\left[\frac{g\alpha\Delta T d^3}{\kappa\nu}\right]^{\beta} \tag{4}$$

$$=\frac{2k\Delta T_u}{d}A\left[2\Delta T_u\frac{g\alpha d^3}{\kappa\nu}\right]^{\beta}. \tag{5}$$

In Eq. (5), the heat flux is expressed in terms of the average temperature drop ΔT_u across the upper boundary layer. In the absence of external forcing, $\Delta T_u=\Delta T/2$ and Eq. (5) is a trivial result. If the two boundary layers can be analyzed independently, though, Eq. (5) should also apply to the perturbed case ($v_s\neq0$), where $\Delta T_u>\Delta T/2$. Then, a change in the behavior of the lower boundary layer is manifested as a change in ΔT_u. No assumptions are required about the particular mechanism controlling the heat flux across the bottom boundary layer, as long as the temperature difference across the top is known.

If we divide Eq. (5) by the conductive heat flux, we obtain a prediction for the enhancement of Nu as a function of ΔT_u:

$$\frac{\mathrm{Nu}}{\mathrm{Nu}(0)}=\left[\frac{2\Delta T_u}{\Delta T}\right]^{\beta+1}. \tag{6}$$

This prediction (with $\beta=0.28$) is plotted in Fig. 12, along with experimental data derived from Fig. 11. It should be noted that there are no fitted parameters in the prediction. The agreement between the prediction of Eq. (6) and the experimental data indicates that perturbations of the lower boundary layer do not affect the relation between the heat flux and the temperature drop across the upper boundary layer.

We can use a similar approach to analyze the effects of the artificial velocity enhancements on the *lower* boundary layer. Experimentally, the heat flux across the lower boundary layer is determined by a flow velocity v_s and a temperature drop $\Delta T_l\equiv\Delta T-\Delta T_u$, while the upper boundary layer remains unperturbed with a "normal" convective velocity and a temperature drop ΔT_u. According to the analysis described above, the absence of perturbations of the upper boundary layer does not affect the relation between H and ΔT_l. The heat flux would therefore be equivalent if the upper boundary layer were also perturbed with enhanced flow velocities v_s and a temperature drop of ΔT_l. The Rayleigh number for the second case would be lower than that for the first case, though, since the total temperature difference would be $\Delta T_l+\Delta T_l(<\Delta T)$.

We determine the variation of Nu with the Rayleigh number with *both* boundary layers perturbed from our data by defining an *effective Rayleigh number*

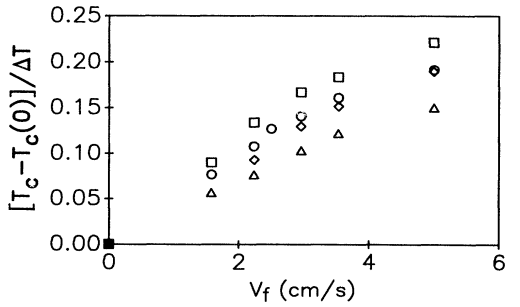

FIG. 11. Shift of the mean center temperature T_c from the unperturbed value $T_c(0)$ as a function of the forcing velocity v_f: $\mathrm{Ra}=3.0\times10^6$ (○), $\mathrm{Ra}=7.8\times10^6$ (△), $\mathrm{Ra}=5.0\times10^7$ (□), $\mathrm{Ra}=1.0\times10^8$ (◇). The shift in T_c is scaled by the total temperature difference ΔT.

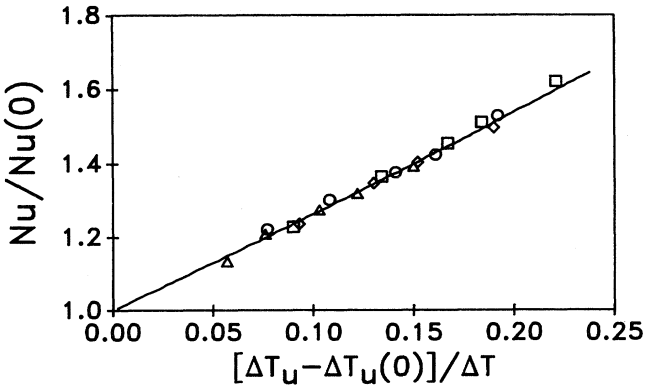

FIG. 12. The Nu enhancement (divided by the unforced Nu) as a function of the normalized shift of the temperature drop ΔT_u across the upper boundary layer. The symbols are the same as in Fig. 11. The solid curve is the prediction of Eq. (6). The good agreement demonstrates the independence of the two boundary layers.

$$\mathrm{Ra}_{\mathrm{eff}}=\frac{2\Delta T_l}{\Delta T}\mathrm{Ra} \tag{7}$$

for each data point. We examine the variation of Nu with $\mathrm{Ra}_{\mathrm{eff}}$ rather than Ra in the following section.

B. Scaling relation for the forced Nusselt number

The enhancement of Nu by artificial boundary-layer velocities (Fig. 9) can be expressed as a function of both v_s and $\mathrm{Ra}_{\mathrm{eff}}$. This function is determined by choosing appropriate Rayleigh number-dependent normalizations for Nu and v_s that will make the data collapse onto a single curve. For the velocity normalization, we use a characteristic "free-fall" velocity v_{FF}, where

$$v_{\mathrm{FF}}=(\tfrac{1}{2}g\alpha\Delta T d)^{1/2}=(\tfrac{1}{2}\mathrm{Ra}\,\mathrm{Pr})^{1/2}\frac{\kappa}{d}\ . \tag{8}$$

This is an *idealized* velocity scale, obtained by assuming that plumes with the average boundary layer temperature fall (or rise) the height of the cell with an acceleration $g\alpha\Delta T/4$. Actual convective velocities are an order of magnitude smaller than v_{FF} in the range of Ra studied in these experiments. (See Refs. 4 and 32 for experimental measurements of typical convective velocities.)

A normalization for Nu is chosen by determining the variation of Nu with $\mathrm{Ra}_{\mathrm{eff}}$, holding v_s/v_{FF} fixed. Assuming a power-law dependence as a hypothesis, a scaling exponent consistent with 1/3 (to within ±0.02) is found for each v_s/v_{FF} examined. This result suggests that normalization of Nu by a function that varies as $\mathrm{Ra}_{\mathrm{eff}}^{1/3}$ will cause the heat-flux data to collapse onto a single curve. For this reason, we have chosen the classical prediction $\mathrm{Nu}_{\mathrm{cl}}$ [Eq. (2)] for the heat-flux normalization. In Fig. 13, $\mathrm{Nu}/\mathrm{Nu}_{\mathrm{cl}}$ is plotted as a function of v_s/v_{FF}, with both $\mathrm{Nu}_{\mathrm{cl}}$ and v_{FF} expressed in terms of $\mathrm{Ra}_{\mathrm{eff}}$. Adjustments have been made to correct for the aspect ratio dependence of the tall cell ($d=9.0$ cm) data.[33] When plotted in this manner, the data collapse onto a curve that can be described (over the accessible range) by the scaling relation

$$\frac{\mathrm{Nu}}{\mathrm{Nu}_{\mathrm{cl}}}=2.9\left[\frac{v_s}{v_{\mathrm{FF}}}\right]^{0.28}, \tag{9}$$

with scaling exponent $\xi=0.28\pm0.01$. [It is probably coincidental that the exponent ξ in Eq. (9) is approximately equal to β.] This expression summarizes the effects of the boundary-layer forcing for various Ra and v_s over the accessible range of these experiments, though other functional forms may also be devised to fit the data.

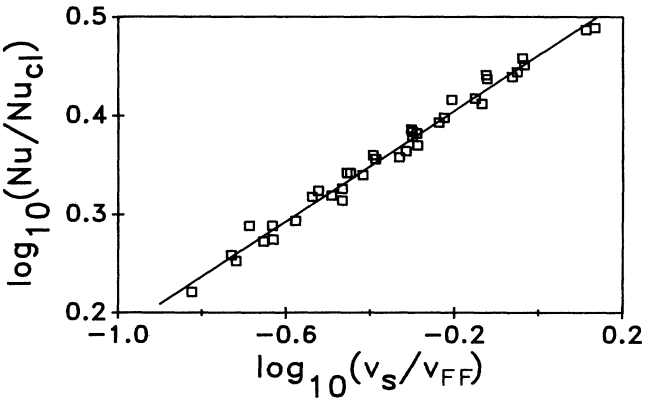

FIG. 13. Enhancement of the heat flux by external forcing as a function of the strength v_s of the induced secondary flow. The data is adjusted to correspond to the forcing of both boundary layers. The effective Rayleigh number $\mathrm{Ra}_{\mathrm{eff}}$ [Eq. (7)] varies from 10^6 to 10^8. The Nusselt number Nu is scaled by the classical prediction [Eq. (2)], and v_s is scaled by the free-fall velocity v_{FF} [Eq. (4)]. The data collapse onto a single curve with slope 0.28 ± 0.01.

VI. DISCUSSION AND CONCLUSION

Our most important conclusion is that the nonclassical scaling of the heat flux with Rayleigh number *without* forcing, and its larger magnitude compared to the classical prediction at moderate Ra, are due to advection of heat from the boundary layer by large-scale flows. These results are generally consistent with the approach of Ref. 8, though the Reynolds number is somewhat lower than assumed in that work. The evidence for this conclusion is developed in the following paragraphs.

We have seen that the thermal boundary layers are controlled by a balance of advective and diffusive heat flux (with $\mathrm{Nu}>\mathrm{Nu}_{\mathrm{cl}}$), rather than by marginal stability, if recirculating flows of sufficient strength are present (Sec. IV B). In our "many-vortex" forcing experiments, we essentially measured the recirculating flows required to produce a given heat-flux enhancement. We can use these measurements to estimate the large-scale flows required to account for the increase of Nu above $\mathrm{Nu}_{\mathrm{cl}}$ in the *unperturbed* case and compare this estimate with experiment. To do this, we first note that the power-law fit for Eq. (9) assumes that the external forcing dominates the velocity field in the vicinity of the lower boundary layer, as was discussed in Sec. III D. Obviously, Eq. (9) is not valid for small v_s, where natural large-scale flows near the boundary layer with typical velocity v_b are significant. We propose that the quantitative effects of v_b are similar to those of v_s, and let v_b replace v_s in Eq. (9).

A semiquantitative comparison can easily be made at $\mathrm{Ra}=10^8$ where $\mathrm{Nu}/\mathrm{Nu}_{\mathrm{cl}}=1.52$. We use Eq. (9) to estimate that $v_b\cong0.15$ cm/s would be required to account for the unperturbed heat flux.[34] *Such a flow is in fact quite consistent with measurements of the flows present spontaneously near the boundary layer,* about 0.1–0.2 cm/s at $\mathrm{Ra}=10^8$ and cell depth $d=9.0$ cm.

The forcing experiments and the nonclassical heat-flux exponent β allow some information to be gleaned speculatively about the growth of v_b with Ra. We rewrite Eq. (9) as

$$\mathrm{Nu}\sim\mathrm{Ra}^{(1/3-\xi/2)}v_b^{\xi}\ . \tag{10}$$

Here, we have made the substitutions $\mathrm{Nu}_{\mathrm{cl}}\sim\mathrm{Ra}^{1/3}$ and $v_{\mathrm{FF}}\sim\mathrm{Ra}^{1/2}$. Inserting $\mathrm{Nu}\sim\mathrm{Ra}^{\beta}$ and postulating a scaling law $v_b\sim\mathrm{Ra}^{\zeta}$ for the boundary-layer velocity in the unperturbed case, we find

$$\zeta=\tfrac{1}{2}+(\beta-\tfrac{1}{3})/\xi\ . \tag{11}$$

The experimental values $\beta=0.28$ and $\xi=0.28$ then imply that $\zeta\cong 0.31$.

Unfortunately, direct measurements of v_b as a function of Ra were not made in these experiments. We note that the exponent ζ deduced indirectly is significantly smaller than that for velocities in the *interior* of the convecting layer as measured in other experiments[4,32] and predicted theoretically in Ref. 8. However, the scaling may well depend on the height at which the velocity is measured (especially in the vicinity of the boundary layers), and we cannot be certain that the spontaneous large-scale flows v_b have precisely the same effects as the induced secondary flows v_s. Therefore, we believe that the relatively low value of ζ estimated above does not detract significantly from the evidence for advection by large-scale flows.

These experiments over a limited range in Rayleigh number generally support the notion that both the magnitude and the anomalous scaling exponent for the heat flux (without forcing) may be explained by recirculating flows that advect heat from the boundary layer. Measurements of the velocity and temperature fields near the boundary layer would provide further insight into these issues.

ACKNOWLEDGMENTS

We are pleased to acknowledge useful discussions with J. Domaradzki, P. Friedman, B. Shraiman, and E. Siggia. Our work on turbulent convection was stimulated originally by discussions with S. Zaleski. The assistance of T. Davis in the construction of the convection apparatus is gratefully acknowledged. This work was supported by the University Research Initiative program under Contract No. DARPA/ONR N00014-85-K-0759.

APPENDIX: SOFT VERSUS HARD TURBULENCE—COHERENCE OF PLUMES

The ability to perturb the thermal boundary layers and to alter the resulting eruptions allows us to study the effect of the plume structure on the transition between soft and hard turbulence. Before discussing the forced case, we note some differences and similarities between our experimental observations without external forcing and those of Ref. 10. First, we do not observe a transition in the scaling exponent β in the (limited) Rayleigh-number range studied. Various other experiments[13–17] that have measured the scaling of Nu with Ra in the same range claim similar results (i.e., no transition in β). For this reason, we distinguish the soft and hard regimes only by the functional form of the temperature probability distribution functions (PDF's) measured in the center of the cell.

As we explained in a previous paper,[9] the center PDF's for $\mathrm{Ra}>3\times10^7$ in this experiment are exponential, like those of the hard turbulence regime of Ref. 10. For $\mathrm{Ra}\lesssim 10^7$, however, the center PDF's are "mixed," having Gaussian tails and exponential peaks. The difference in the functional form of these PDF's and those of the soft turbulence regime of Refs. 10 and 6 (which do not have exponential peaks) is apparently due to the aspect ratio of the convecting layer (Fig. 14). At an aspect ratio of 1.6 [Fig. 15(a)], the PDF's for $\mathrm{Ra}\lesssim 10^7$ are mixed, whereas at a smaller aspect ratio [Fig. 15(b)], the PDF's in the same Ra range are fully Gaussian. *Thus the PDF's at low Ra do not have a universal form and depend on aspect ratio.* If the aspect ratio is small, most of the plumes pass through the probe, whereas they often miss the probe for the larger aspect ratio. In the latter case, the probability at the average cell temperature is increased, so the overall

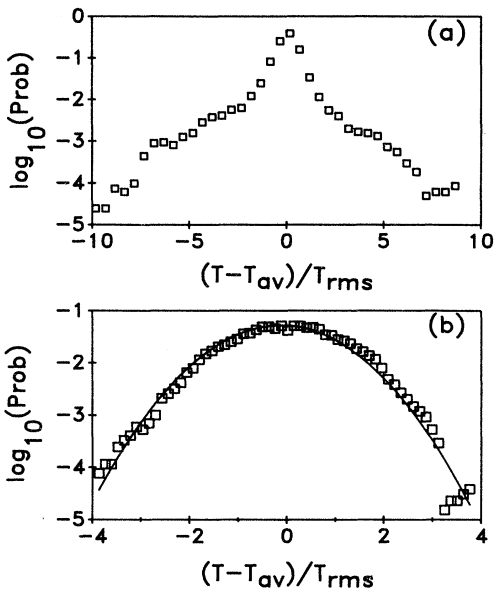

FIG. 14. Dependence of the center probability distribution function (PDF) on aspect ratio for soft turbulence. (a) Aspect ratio $\Gamma=1.6$, $\mathrm{Ra}=4.9\times10^6$. The PDF is mixed, having Gaussian tails but exponential peaks. (b) $\Gamma=0.7$, $\mathrm{Ra}=5.4\times10^6$. The PDF is Gaussian. The aspect ratio of the cell has been reduced in (b) by adding Plexiglass spacers to the interior of the small ($d=4.0$ cm) cell.

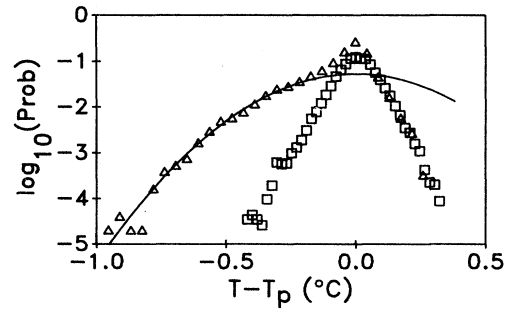

FIG. 15. Transition in the center probability distribution function (PDF) induced by single-vortex forcing at $\mathrm{Ra}=1.2\times10^8$. The cases shown are unperturbed (□) and forced with $v_f=5.7$ cm/s (△). The peak temperature T_p has been subtracted from the temperature axis. The tails of the PDF are fitted to an exponential in the unforced (□) case and to a Gaussian in the forced (△) case. The transition in the PDF is associated with more coherent plumes.

behavior is non-Gaussian.

We find that the difference between the PDF's of the soft and hard turbulent regimes is related to the coherence of thermal plumes in the interior of the flow, as suggested by Domaradzki.[35,9] Observations of the temperature field in unperturbed convection with thermochromic liquid-crystal (TLC) visualization show that at lower Ra (soft turbulence), plumes emitted from the boundary layers frequently span the full height of the cell.[9] Large plumes result in slowly varying time series, associated with Gaussian tails in the PDF's. At higher Ra in the hard turbulence regime, the plumes are broken into smaller structures before traversing the cell, either as a result of the stronger interior winds or the larger layer depth. The smaller thermal structures result in spiky time series, which correspond to the exponential PDF's.

This interpretation is further supported by changes in the PDF's measured at the center probe in the presence of a single time-independent forcing vortex at $Ra=1.2\times10^8$ (Fig. 15). A transition is induced in the form of the PDF by the forcing flow, which suppresses warm eruptions from the lower boundary layer and enables cool plumes from the top to remain coherent as they fall to the bottom. The center PDF, which is exponential in the unperturbed case, then has a Gaussian tail on the cool side while the warm excursions are unaffected. Thus, *the various observations indicate that the coherence of plumes determines the form of the PDF's.*

Improved characterization of the temperature fields would probably clarify the relationship between spatial thermal structures and probability distribution functions measured at a point. Studies of this nature may be practical with the thermochromic liquid crystal technique.

---

*Present address: Center for Nonlinear Dynamics, University of Texas, Austin, TX 78712.

[1]W. V. R. Malkus, Proc. R. Soc. London Ser. A **225**, 196 (1954).

[2]L. N. Howard, in *Proceedings of the 11th International Congress of Applied Mechanics, Munich, Germany* (Springer, Berlin, 1966).

[3]R. Krishnamurti and L. Howard, Proc. Natl. Acad. Sci. **78**, 1981 (1981); J. Fluid Mech. **170**, 385 (1986).

[4]M. Sano, X. Z. Wu, and A. Libchaber, Phys. Rev. A **40**, 6421 (1989).

[5]T. Asaeda and K. Watanabe, Phys. Fluids A **1**, 861 (1989).

[6]B. Castaing, G. Gunaratne, F. Heslot, L. Kadanoff, A. Libchaber, S. Thomae, X. Z. Wu, S. Zaleski, and G. Zanetti, J. Fluid Mech. **204**, 1 (1989).

[7]S. Zaleski (private communication).

[8]B. Shraiman and E. Siggia, Phys. Rev. A **42**, 3650 (1990).

[9]T. H. Solomon and J. P. Gollub, Phys. Rev. Lett. **64**, 2382 (1990).

[10]F. Heslot, B. Castaing, and A. Libchaber, Phys. Rev. A **36**, 5870 (1987).

[11]S. Gross, G. Zocchi, and A. Libchaber, C. R. Acad. Sci. Paris **307**, 447 (1988).

[12]G. Zocchi, E. Moses, and A. Libchaber, Physica A **166**, 387 (1990).

[13]E. F. C. Somerscales and I. W. Gazda, Int. J. Heat Mass Transfer **12**, 1491 (1969).

[14]T. Y. Chu and R. J. Goldstein, J. Fluid Mech. **60**, 141 (1973).

[15]D. C. Threlfall, J. Fluid Mech. **67**, 17 (1975).

[16]D. E. Fitzjarrald, J. Fluid Mech. **73**, 693 (1976).

[17]H. Tanaka and H. Miyata, Int. J. Heat Mass Transfer **23**, 1273 (1980).

[18]R. J. Goldstein, H. D. Chiang, and D. L. See, J. Fluid Mech. **213**, 111 (1990).

[19]S. Zaleski, in *The Global Geometry of Turbulence* (Plenum, New York, 1990).

[20]J. Sommeria, J. Fluid Mech. **170**, 139 (1986).

[21]P. Tabeling, B. Perrin, and S. Fauve, Europhys. Lett **3**, 459 (1987).

[22]These secondary flows were suppressed in Ref. 9 by using time-periodic electric currents. The resulting flow enhancements are then almost strictly horizontal.

[23]T. H. Solomon, Ph.D. dissertation, University of Pennsylvania, 1990.

[24]T. S. Sudarshan, M. H. Lim, P. L. Hefley, and J. E. Thompson, J. Appl. Phys. **56**, 2236 (1984).

[25]B. B. Damaskin and O. A. Petrii, *Adsorption of Organic Compounds on Electrodes* (Plenum, New York, 1971).

[26]T. Smith, Advan. Colloid Interface Sci. **3**, 161 (1972).

[27]This is accomplished by inserting the stainless-steel tube into the cell until the end just touches the interface. The bore of the syringe is pulled back, drawing mercury, water and impurities into the syringe. The syringe contents are then dumped into a container, in which the water and impurities rise to the top. Clean mercury at the bottom of the container can then be recovered and injected back into the cell. The process is repeated until the interface shows no traces of contamination.

[28]H. S. Rhee, J. R. Koseff, and R. L. Street, Exp. Fluids **2**, 57 (1984); D. Dabiri and M. Gharib, Bull. Am. Phys. Soc. **34**, 2337 (1989); Exp. Fluids (to be published).

[29]The microspheres were obtained from Hallcrest, 1820 Pickwick Lane, Glenview, Illinois 60025.

[30]R. J. Emrich, in *Methods of Experimental Physics,* edited by L. Marton and C. Marton (Academic, New York, 1981).

[31]R. H. Kraichnan, Phys. Fluids **5**, 1374 (1962).

[32]H. Tanaka and H. Miyata, Int. J. Heat Mass Transfer **23**, 1273 (1980).

[33]For the tall cell, Nu was reduced by 16% in Fig. 13.

[34]This estimate is made for the $d=9.0$ cm cell, for which the coefficient in Eq. (9) must first be muliplied by 1.16 to remove the aspect ratio adjustment.

[35]J. A. Domaradzki (private communication).

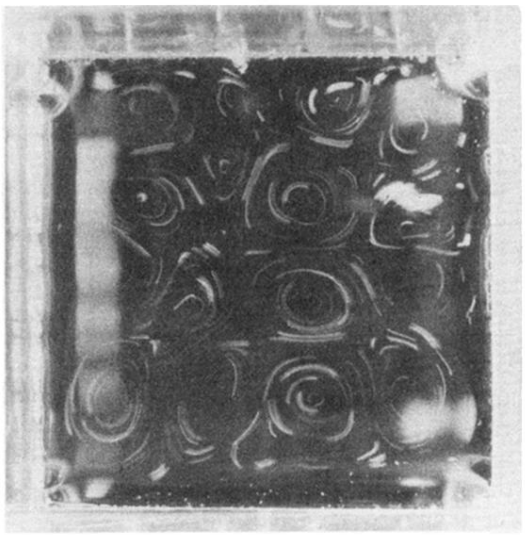

FIG. 2. Time exposure of the mercury flow with many-vortex forcing. The maximum velocity, as determined by particle streak photography, is 1.6 cm/s.